IEEE Access
Multidisciplinary ⋮ Rapid Review ⋮ Open Access Journal

Received 19 December 2023, accepted 30 December 2023, date of publication 2 January 2024,
date of current version 9 January 2024.

Digital Object Identifier 10.1109/ACCESS.2023.3349348

RESEARCH ARTICLE

A Low-Complexity Compressive Sensing Algorithm for Point Target Detection Using Ultrafast Plane Wave Imaging

ROYA PARIDAR AND BABAK MOHAMMADZADEH ASL, (Member, IEEE)
Department of Biomedical Engineering, Tarbiat Modares University, Tehran 14115-111, Iran
Corresponding author: Babak Mohammadzadeh Asl (babakmasl@modares.ac.ir)

ABSTRACT Ultrasound plane wave imaging is an ultrafast technique to obtain the reconstructed images in real-time. However, identifying the point targets (such as microcalcifications) is challenging in this imaging technique due to the presence of strong acoustic clutter. In this paper, a compressive sensing (CS)-based algorithm, named modified-CS (M-CS), is proposed which can be used to accurately identify the point targets. In the proposed algorithm, the processing matrix is divided into some non-overlapping sub-matrices, and each part is processed separately. Then, the output passes through the thresholding and localization processes to obtain the locations of the point targets. Compared to the conventional CS algorithm, identifying the point targets in deeper regions of the imaging medium is provided using the M-CS algorithm. Also, due to the usage of smaller sub-matrices, the proposed M-CS algorithm speeds up, and also, needs less memory compared to the conventional CS algorithm. The simulation results confirm the good performance of the proposed algorithm.

INDEX TERMS Ultrasound, ultrafast imaging, sparsity, point detection.

I. INTRODUCTION

Ultrasound imaging is a commonly used technique in the medical field that attracts a lot of attention due to its non-ionizing and real-time properties. This imaging technique is used in diagnosis and treatment applications [1]. In particular, ultrasound imaging can be used in the early detection of breast cancer; identifying the microcalcifications, i.e., point-like calcium particles that are distributed in the breast tissue, is helpful in diagnosing whether the breast cancer is benign or malignant. Note that the microcalcifications reflect strong waves due to their large impedance differences compared to their surrounding soft tissue. Therefore, they appear as point targets in the reconstructed ultrasound image [2]. The number, distribution, and even the shape of the microcalcifications are informative in order to diagnose the disease [3]. It can be concluded that ultrasound imaging with the aim of revealing point targets in the tissue is applicable. Kidney stone identification, tracking the moving point-like particles in the tissue (e.g., microbubble imaging), and also, needle tracking during the biopsy process are other examples of the applications of point target identification in medical ultrasound imaging [4], [5].

TABLE 1. List of abbreviations that are used in this paper.

Abbreviation	Full writing
CF	Coherence Factor
CS	Compressive-Sensing
CPWC	Coherent Plane Wave Compounding
DAS	Delay-And-Sum
GCF	Generalized Coherence Factor
i.i.d	independent and identically distributed
M-CS	Modified Compressive-Sensing
MV	Minimum Variance
PWI	Plane Wave Imaging
ROC	Receiver Operating Characteristic
SLSC	Short-Lag Spatial Coherence

Different algorithms can be used to reconstruct the image and reveal the point targets. The data-independent

The associate editor coordinating the review of this manuscript and approving it for publication was Fang Yang.

delay and sum (DAS) algorithm is the most common beamformer. Although this algorithm is simply implemented, the result strongly suffers from poor resolution and contrast. The data-dependent minimum variance (MV) algorithm and its improved versions such as forward-backward and eigenspace-based MV algorithms, improve the image resolution by weighting the received signal adaptively [6], [7], [8], [9]. Therefore, a better separation of two close point targets will be achieved compared to DAS. Other techniques such as the coherence factor (CF) and generalized CF (GCF) weighting methods have also been developed to suppress the noise level and improve the detection capability [10]. However, point target identification using the mentioned algorithms is still a challenge due to the strong effect of acoustic clutter on ultrasound imaging. In order to overcome this limitation and identify the point targets within the tissue in the presence of strong clutter, various studies have been conducted so far. A list of related works is presented in the following; in [11] and [12], an algorithm known as the Bayesian information criteria was presented to identify the point targets in the ultrasound image through an iterative process, and it was shown that this algorithm outperforms DAS and MV beamformers. In [13], two binary microcalcification mapping techniques were developed using the CF weighting method, and also, the first eigenvalue of the covariance matrix of the beamformed data. The outputs of these algorithms were overlaid on the B-mode image to determine the distribution of microcalcifications. In [14], a coherence-based wavelet coefficient shrinkage method was proposed in order to suppress the background speckle and increase the probability of point target identification. In [15], a correlation-based method known as the excitelet method was proposed which leads to resolution improvement and artifact reduction of the final image. This is achieved by considering the correlation between the reference signal and the measured signals obtained from the array. In [16], the combination of multi-line and short-lag spatial coherence (SLSC) methods is used to suppress the clutter and better reveal the point targets. In [17], a multilook-based technique was developed to increase the probability of detection. In this algorithm, the pre-whitening method was also used to improve the SNR and further suppress the noise level. Some image reconstruction algorithms, such as SLSC, in coherent plane wave compounding (CPWC) have also been evaluated in [18] in kidney stone identification.

It is well-known that by using the compressive sensing (CS) algorithm, an improved contrast reconstructed image will be obtained [19], [20], [21]. In this algorithm, by taking this assumption into account that the data is sparse, much smaller samples compared to the Nyquist rate are used to efficiently construct the final image. As the CS algorithm efficiently suppresses the noise level [22], [23], it is expected that by using this method, point targets are extracted more successfully from the background speckle, and a more accurate identification will be achieved.

In this paper, it is proposed to use the CS algorithm in plane wave imaging (PWI) to identify point targets; on one hand, by using the PWI, high frame rate (ultrafast) imaging is possible [24], [25]. On the other hand, the image quality will be degraded in PWI compared to focused ultrasound imaging due to the usage of unfocused transmitted beams, which negatively affects the point target identification. Note that the image quality is improved by coherently compounding the received signals corresponding to multiple emissions from different angles, i.e., the so-called CPWC technique [26]. However, there is a trade-off between the image quality and frame rate in CPWC. Also, point detection still remains a challenge due to low signal-to-noise ratio and strong acoustic clutter. It has been shown that the CS algorithm significantly suppresses the noise, and consequently, improves the image contrast in PWI [27]. Also, it has been shown that a limited number of emissions (one or two) is sufficient for the CS algorithm to reach its best performance [28]. As a result, by processing the received signals obtained from only a single emission in plane wave imaging, the point targets will be successfully identified while the frame rate is not degraded. One should note that the drawback of the CS algorithm is that the point detection ability will be lost by increasing the imaging depth [22]. To tackle this problem, a modified CS (M-CS) algorithm is proposed in this paper that leads to efficiently identifying the point targets even in deep regions. Our contributions are summarized below:

- A CS-based algorithm is used to identify the point targets in CPWC. In the proposed method, the algorithm is performed only on the received signals corresponding to the middle emission (0°). Once the locations of point targets are identified, they are overlaid on the B-mode image obtained from the CPWC process to determine the positions of point targets within the tissue.
- In order to make it possible to identify the point targets in deeper regions of the imaging medium using the CS-based algorithm, the M-CS algorithm is developed. By using the proposed algorithm, the limitations of the CS algorithm are overcome. Also, note that in the M-CS algorithm, the matrix to be processed is divided into a number of sub-matrices, each of which is processed independently. Therefore, in addition to reducing the memory required to process each sub-matrix, the process can be done in parallel. Consequently, the computational burden will be reduced.

The rest of the paper is organized as follows. The CPWC technique as well as the CS algorithm are briefly explained in Section II. The proposed method is presented in Section III. The results obtained from the simulation study are evaluated in Section IV. Finally, the discussion and conclusion are provided in Sections V and VI, respectively. The list of abbreviations that are used in the paper is presented in Table 1 to find their corresponding full writing more easily.

II. BACKGROUND

In this section, image reconstruction using the non-adaptive DAS beamformer as well as the conventional CS algorithm are briefly discussed in CPWC. Then, inspired by the CS algorithm, the proposed method will be presented in Section III.

A. COHERENT PLANE WAVE COMPOUNDING

In CPWC, N_p tilted plane waves are used to insonify the imaging medium from different emission angles. Then, the received signals corresponding to each emission are acquired and processed to obtain the final reconstructed image. In particular, with the consideration of an N_e-element linear array, the DAS beamformed data corresponding to j^{th} emission is obtained as below:

$$\begin{aligned} y^{(j)}_{\mathrm{DAS}}(n) &= \sum_{i=1}^{N_e} s_{i,j}(n - \tau_{i,j}(n)) \\ &= \sum_{i=1}^{N_e} x_{i,j}(n) \quad \text{for } j = 1, \cdots, N_p, \end{aligned} \tag{1}$$

where $s_{i,j}(n)$ denotes the received signal corresponding to i^{th} element and j^{th} emission for n^{th} imaging point. Also, $\tau_{i,j}(n)$ is the time delay proportional to the round-trip path of the wave corresponding to i^{th} element and j^{th} emission which is applied to the received signal in order to perform focusing on the n^{th} imaging point [26]. The time-delayed signal associated with the i^{th} element and j^{th} emission is denoted as $x_{i,j}(n)$. By processing the received signals obtained from each emission, the low-quality images will be reconstructed. By coherently compounding the low-quality images, improved image quality in terms of both resolution and contrast will be achieved. More precisely, the final reconstructed image in CPWC is obtained as below:

$$\begin{aligned} y_{\mathrm{DAS}}(n) &= \frac{1}{N_p} \sum_{j=1}^{N_p} y^{(j)}_{\mathrm{DAS}}(n) \\ &= \frac{1}{N_p} \sum_{j=1}^{N_p} \sum_{i=1}^{N_e} x_{i,j}(n), \end{aligned} \tag{2}$$

which is obtained from the DAS algorithm.

B. COMPRESSIVE SENSING ALGORITHM

In the CS algorithm, the reconstructed image is obtained by using much fewer samples compared to the Nyquist rate. The CS problem is formulated as below:

$$\boldsymbol{s}_{i,j} = \boldsymbol{A}(i,j)\boldsymbol{y}^{(j)} + \boldsymbol{n}, \tag{3}$$

where $\boldsymbol{s}_{i,j} \in \mathbb{C}^{M\times 1}$ denotes the received signal consisting of M samples which corresponds to i^{th} element and j^{th} plane wave. Considering that the final reconstructed image is represented in a $N_x \times N_y$ grid, $\boldsymbol{y}^{(j)} \in \mathbb{C}^{N_xN_y\times 1}$ is the solution of the above problem which we are looking for, i.e., the (reshaped) reconstructed image. Also, $\boldsymbol{n} \in \mathbb{C}^{M\times 1}$ is noise and $\boldsymbol{A}(i,j) \in \mathbb{C}^{M\times N_xN_y}$ is the measurement matrix corresponding to i^{th} element and j^{th} emission. Note that the measurement matrix is designed based on the imaging geometry and independently of the data; that is, for a fixed imaging geometry, the measurement matrix can be designed once, and used to reconstruct the images of different imaging objects. In this study, the measurement matrix is designed according to the following equation [29], [30]:

$$a_{mn}(i,j) = \begin{cases} 1 & \text{for } f_s \left|\boldsymbol{\tau}_{i,j}(n) - t_m\right| < 1 \\ 0 & \text{else,} \end{cases} \tag{4}$$

where $a_{mn}(i,j)$ denotes the m^{th} row and n^{th} column of the matrix $A(i,j)$, f_s is the sampling frequency, and t_m represents the temporal measurement associated with the m^{th} sample. Considering the prior knowledge about the sparsity of $\boldsymbol{s}_{i,j}$, the reconstructed image is obtained by solving the following minimization problem:

$$y^{(j)}_{CS} = \underset{y^{(j)}_{CS}}{argmin} \left\|A(i,j)\boldsymbol{y}^{(j)}_{CS} - s_{i,j}\right\|_2^2 + \alpha \left\|y^{(j)}_{CS}\right\|_1, \tag{5}$$

where $y^{(j)}_{CS}$ is the obtained solution corresponding to j^{th} emission which should be reshaped as $\boldsymbol{Y}^{(j)}_{CS} \in \mathbb{C}^{N_x\times N_y}$ in order to visualize the image. Also, $\|.\|_p$ denotes the ℓ_p-norm regularization term, and $\alpha \in [0, 1]$ is a constant that determines the participation of the sparse regularization term $\left\|y^{(j)}_{CS}\right\|_1$. Note that in the case where the data is non-sparse, one can inspire a transformation matrix in order to achieve a sparse representation of the data and use it to solve the problem [23]. This topic is out of the scope of this paper, and therefore, will not be investigated.

III. PROPOSED METHOD

In this paper, the M-CS algorithm is proposed to identify point targets in ultrafast imaging. The reconstructed images obtained from the PWI suffer from poor quality (especially in terms of contrast) compared to the focused imaging technique due to unfocused emissions. This negatively affects the point target identification process. The CS algorithm significantly suppresses the noise level and improves the image contrast by using the received signals corresponding to a limited number of emissions (one or two). Therefore, it can be concluded that the CS algorithm helps the point targets to be better identified. However, there are two main limitations to this algorithm:

- The dimensionality of the matrix to be processed is usually high; a $M \times N_xN_y$ matrix should be constructed during the process according to (5). As the imaging region, and consequently, the number of pixels that are included in the final image increases, a greater memory is required to perform the process and obtain the reconstructed image.
- As the value of the parameter α increases, better noise suppression is achieved. As a result, the point targets will be better identified and separated from the background speckle. However, the information corresponding to the

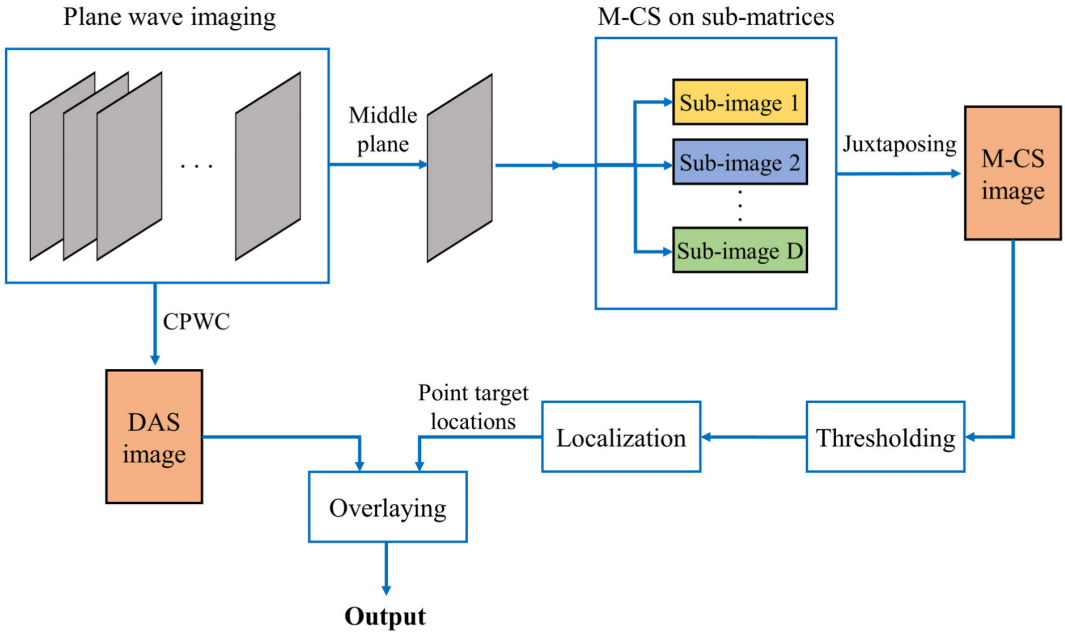

FIGURE 1. The schematic of the proposed point detection method.

deeper regions of the imaging medium will be lost. This issue was previously evaluated in [22]. Therefore, one can conclude that for a smaller value of α, the probability of error increases such that some scatterers will be identified as point targets. Also, as the value of this parameter increases, point targets in deep regions will not be identified.

In order to overcome the limitations mentioned above, we propose to divide the matrix $\boldsymbol{A}$ and the reconstructed image $\boldsymbol{y}_{CS}^{(j)}$ (presented in (5)) into D non-overlapping parts, and process each part separately. In other words, (5) is reformulated as below:

$$y_{CS_d}^{(j)} = \underset{y_{CS_d}^{(j)}}{argmin} \left\| A_d(i,j)\boldsymbol{y}_{CS_d}^{(j)} - s_{i,j} \right\|_2^2 + \alpha \left\| y_{CS_d}^{(j)} \right\|_1, \quad (6)$$

where $A_d(i,j) \in \mathbb{C}^{M \times \frac{N_x N_y}{D}}$ is the d^{th} measurement sub-matrix the dimensionality of which is $1/D$ times the one presented in the conventional CS algorithm. Also, $\boldsymbol{y}_{CS_d}^{(j)} \in \mathbb{C}^{\frac{N_x N_y}{D} \times 1}$ is the d^{th} part of the reconstructed image. Once the above problem is solved for all the considered D parts, the final reconstructed image is obtained by juxtaposing them as below:

$$\boldsymbol{Y}_{CS}^{(j)} = \begin{bmatrix} \boldsymbol{Y}_{CS_1}^{(j)} \\ \boldsymbol{Y}_{CS_2}^{(j)} \\ \vdots \\ \boldsymbol{Y}_{CS_D}^{(j)} \end{bmatrix}_{N_x \times N_y}, \quad (7)$$

where $\boldsymbol{Y}_{CS_d}^{(j)} \in \mathbb{C}^{\frac{N_x}{D} \times N_y}$ is the d^{th} reconstructed image which is reshaped to form the two-dimensional image. By using the proposed M-CS algorithm, the dimensionality of the processing matrices will be smaller, and therefore, the need for a huge amount of memory is overcome. Also, the effect of the parameter α will start over in each sub-matrix; that is, the problem of information loss in deep regions caused by the parameter α will be tackled. Note that in the proposed method, only the received signals corresponding to the middle emission are considered to be processed using the M-CS algorithm; $j = \lceil N_p/2 \rceil$ is considered in (6), where $\lceil . \rceil$ denotes the upward round operation. Therefore, by using the proposed M-CS algorithm to identify the point targets, not much computational complexity will be imposed.

Once the image is reconstructed using the proposed M-CS method, the following steps are applied to the obtained output in order to identify the locations of the point targets:

1) **Removing small intensities using a threshold:** In this step, the zero value is assigned to some parts of the image, and only the high-intensity pixels, i.e., the regions associated with point targets will remain. This is achieved by using a pre-determined threshold τ.
2) **Finding the local maximum positions:** Once the thresholding process is performed, some local high-intensity regions will appear in the output image. In this step, the maximum point of each region is found and considered as the center position of the point target. This process is inspired by the localization process which is used in super-resolution ultrasound imaging.
3) **Overlaying the target positions on the B-mode image:** The final step is to overlay the identified positions of the point targets on the B-mode image. Note that the B-mode image can be achieved using a limited number of emissions in order to achieve an

overview of where the point targets are located in the tissue.

The processing steps of the proposed algorithm are schematically shown in Fig. 1. Moreover, the pseudocode of the proposed method is presented in **Algorithm 1** to better see the detailed procedure. The procedure described in lines 1-8 of the pseudocode results in the reconstructed image in which the noise level is significantly suppressed. This is while the point targets located at deep regions of the medium are preserved. Note that the process does not occupy much memory thanks to dividing the matrix into some small sub-matrices. The procedure described in lines 9-10 of the pseudocode is also used to identify the exact locations of the point targets. As the noise level is successfully suppressed in the previous stages (i.e., the proposed M-CS algorithm), the performance of the simple thresholding method to identify the locations of the point targets is significantly improved compared to the conventional CS algorithm. Therefore, the probability of identifying the spurious point targets will be low, and most of the existing point targets will be identified.

To better clarify the strengths and weaknesses of the proposed method over other related works that are used in the evaluations, Table 2 is presented. As can be seen from the table, the proposed method overcomes the limitations of the conventional CS algorithm. Also, compared to DAS and MV algorithms, the M-CS method significantly suppresses the noise level which improves the point target identification. Detailed evaluation of the mentioned algorithms will be performed in the following sections.

A. EVALUATION METRICS

The following evaluation metrics are defined and used in order to evaluate the performance of the proposed algorithm in terms of the ability to correctly identify the point targets:

- **Missed detection** evaluation metric, which is defined as the ratio of the number of point targets that are not identified to the total number of existing point targets in the imaging medium.
- **True detection** evaluation metric, which is defined as the ratio of the number of point targets that are correctly identified to the total number of existing point targets in the imaging medium.
- **False detection** evaluation metric, which is defined as the ratio of the number of spurious point targets that are identified by the algorithm to the total number of existing point targets in the imaging medium.

Note that all the mentioned evaluation metrics are in the range of $[0, 1]$. As the values of the missed detection and false detection metrics get smaller, one can conclude that the performance of the algorithm is improved. Also, the greater the value of the true detection metric, the better the performance of the algorithm in terms of revealing the existing point targets.

IV. RESULTS

A simulation study is performed in order to evaluate the performance of the proposed method to identify point targets. The Field II Matlab toolbox is used to perform the simulation [31]. In the designed phantom, a large number of scatterers are uniformly distributed along a $10 \times 40 \times 60$ mm^3 volume to simulate a speckle-generating phantom. Then, 40 point targets (high-reflectors) are randomly placed in the considered volume. The adjusted parameters to perform the simulation are presented in Table 3.

The reconstructed images obtained from the DAS algorithm (using all the N_p emissions), the adaptive MV algorithm, the CS algorithm, and the proposed M-CS method are demonstrated in Fig. 1. Note that the reconstructed images of the algorithms, except the DAS algorithm, are obtained by using only the middle plane wave. Also, in the proposed M-CS algorithm, $D = 8$ is considered. It can be seen that the point targets cannot be well revealed in the reconstructed image obtained from DAS; the background speckle makes it difficult to identify the point targets, especially in deeper regions of the imaging phantom. By using the adaptive MV algorithm, the resolution of the point targets is improved compared to DAS, as demonstrated in Fig. 2 (b). However, identifying the point targets in deep regions is still difficult. Also, the improved resolution of the MV algorithm is achieved at the expense of high computational complexity [439 sec to obtain the reconstructed image shown in Fig. 2 (b)]. The CS algorithm suppresses the background speckle, as shown in Figs. 2 (c-e). Depending on the assigned value of the parameter α, the noise rejection is performed differently in the CS algorithm; the greater the value of α, the more the noise suppression is performed. However, the point targets in deep regions of the imaging medium will be lost. In particular, it can be concluded from Figs. 2 (c-e) that the noise level is better suppressed and the point targets are more clearly visible for $\alpha = 1$. However, the point targets that are located beyond the depth of almost 50 mm are completely disappeared. In contrast, the information in deeper regions of the imaging phantom is not lost for $\alpha < 1$. However, the noise suppression is degraded in such a case, which leads to errors in identifying the locations of the point targets. By comparing the M-CS algorithm (Fig. 2 (f)) and the CS method, it can be seen that the proposed method outperforms the DAS and CS algorithms in terms of noise suppression while the point targets are also revealed even in deep regions of the imaging medium. It should be noted that deep regions of the imaging phantom are still noisy by using the proposed M-CS algorithm, as demonstrated in Fig. 2 (f). This is due to the use of only a single emission without focusing on the imaging points to perform the imaging process (i.e., PWI), which causes a reduction in the energy of the transmitted wave as the imaging depth increases. Consequently, a high level of noise will be induced in the reconstructed image, as can also be seen from Figs. 2 (a-b). By using the conventional CS algorithm, the noise of deep regions is

Algorithm 1 The Processing Steps of the Proposed M-CS Algorithm

Inputs: α, D, τ, N_x, N_y.
Output: Point targets mapping on the B-mode image.
Acquiring the received signals for middle emission, i.e., $\boldsymbol{s}_{i,j}$, for $i = 1, \cdots, N_e$, and $j = \lceil N_p/2 \rceil$.
Constructing the measurement matrix $\boldsymbol{A}$ according to (4).
Dividing the measurement matrix into D sub-matrices, the dimensionality of which equals $M \times \frac{N_x N_y}{D}$.
for $d = 1 : D$ **do**
    Constructing d^{th} part of the image vector by using d^{th} sub-matrix $\boldsymbol{A}_d$ and solving (6).
end
Juxtaposing all the obtained D vector images resulting in a $N_x N_y \times 1$ vector.
Reshaping the vector image into a 2D matrix with the dimensions of $N_x \times N_y$ according to (7).
Omitting the regions the intensities of which exceed the threshold value τ (i.e., $0 \leftarrow y_{CS}^{(j)}(n) \leq \tau$, for $n = 1, \cdots N_x N_y$).
Finding the local maximum intensities and estimating the positions of the point targets.
Overlaying the obtained positions on the B-mode image.

TABLE 2. Comparison of strengths and weaknesses of the algorithms used in the evaluations.

Algorithm	Advantages	Disadvantages
DAS	Low computational complexity	Degraded resolution High level of noise Failure to identify point targets in speckled deep regions
MV	High resolution	High computational complexity Failure to identify point targets in speckled deep regions
CS	High noise suppression Fewer samples requirement compared to Nyquist rate Successful identification of point targets in shallow regions	High computational complexity High memory requirement Degraded performance in deep regions
M-CS	High noise suppression Fewer samples requirement compared to Nyquist rate Successful identification of point targets in shallow and deep regions Low computational complexity Low memory requirement	Limited to point target identification application

TABLE 3. The simulation parameters.

parameter	variable	value
number of elements	N_e	96
number of plane waves	N_p	15
center frequency	f_0	4×10^6 [Hz]
sampling frequency	f_s	20×10^6 [Hz]
sound velocity	c	1540 [m/s]
wavelength	λ	c/f_0 [m]
element height	h_e	5×10^{-3} [m]
kerf	K_e	$\lambda/2$ [m]

eliminated. However, useful information about the imaging medium will also be lost (Figs. 2 (c-e)). Note that by using the proposed method, the amplitude of the point targets is much higher compared to the noisy parts of the reconstructed image in deep regions. Therefore, they can be successfully separated by thresholding which will be discussed in the following.

Once the image is reconstructed, the locations of the point targets are desired to be identified by thresholding and localizing the beamformed data. Then, the identified locations are overlaid on the B-mode image to better visualize the result. The output of the described process is demonstrated in Fig. 3. It can be seen that point detection using the CS algorithm induces error; some spurious point targets are identified, as demonstrated in Fig. 3 (a). As the value of the parameter τ increases, the number of spurious point targets will be reduced. However, some point targets will be lost, as shown in Fig. 3 (b). Finally, it can be seen from Fig. 3 (c) that by using the proposed M-CS method, the point targets are correctly identified.

A. EFFECT OF THE PARAMETERS D AND τ

The proposed method is evaluated for different values of the parameter D and the results are shown in Fig. 4. Note that the results are obtained for $\tau = 0.05$ and $\alpha = 1$. From the missed detection and true detection metrics, one can conclude that the performance of the M-CS algorithm improves for greater values of D; more existing point targets are identified, and the probability of missed detection is reduced. However, the false detection metric is also increased according to Fig. 4 (c), indicating that the number of spurious point targets will be increased as the parameter D increases. This limitation can be overcome by varying the threshold value. To better evaluate the effect of the parameter τ on the performance of the proposed algorithm, pay attention to Fig. 5. It can be

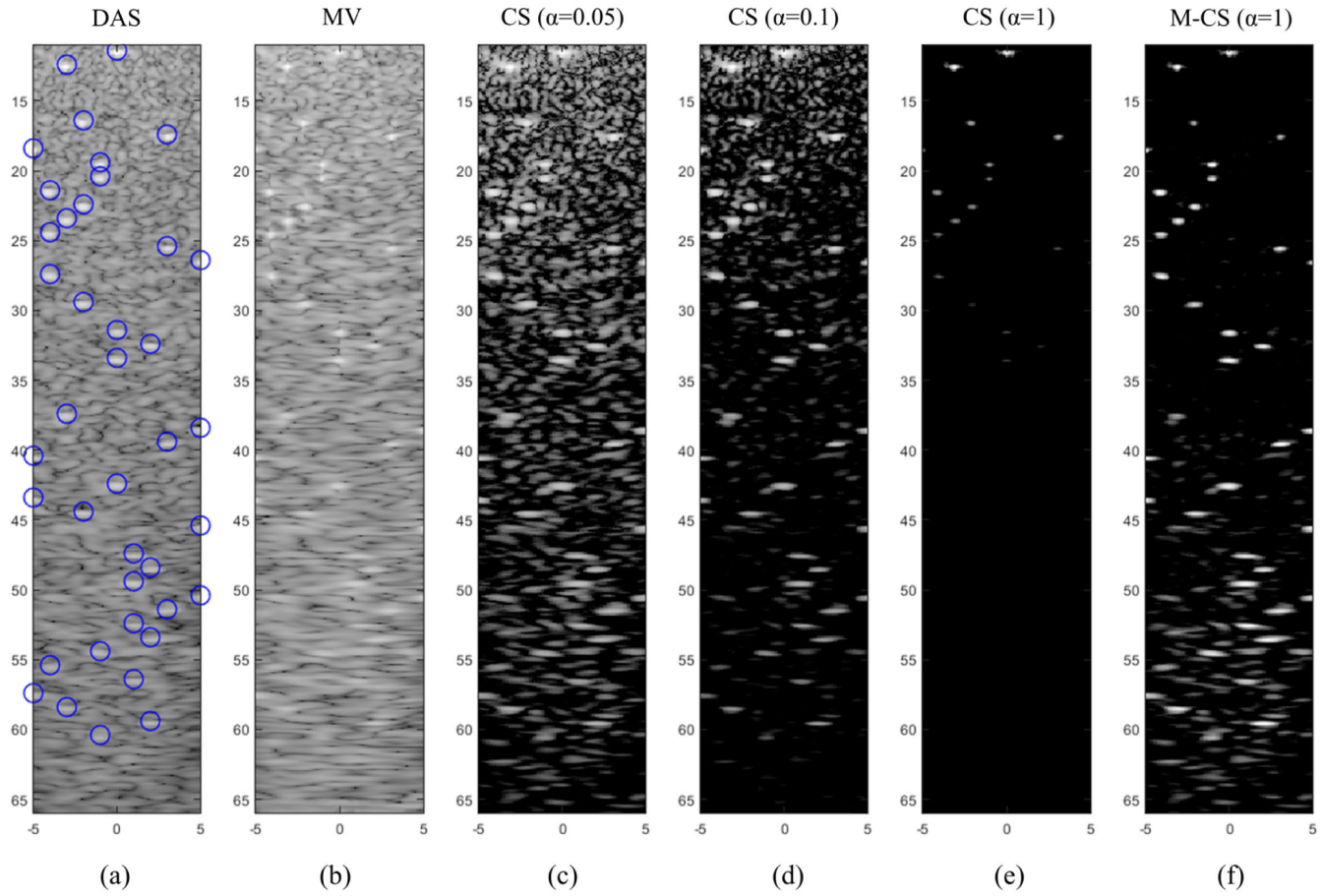

FIGURE 2. Reconstructed images obtained from (a) the DAS algorithm, (b) MV (subarray length equals half the array length), the CS algorithm with (c) $\alpha = 0.05$, (d) $\alpha = 0.1$, (e) $\alpha = 1$, and (f) the proposed M-CS algorithm with $\alpha = 1$ and $D = 8$. The actual locations of the point targets are shown with blue circles in (a). The images are shown with the dynamic range of 70 *dB*.

seen from the figure that as the parameter D increases, the performance of the M-CS algorithm will be improved for greater values of τ. Generally, it can be concluded that the greater the value of D, the better the performance of the M-CS algorithm in terms of identifying the point targets. As the parameter D exceeds a certain value, a greater value should be assigned to τ in order to prevent identifying the spurious point targets. In this simulation study, $D = 8$ leads to the most appropriate performance in which all the point targets are correctly identified. Also, no spurious point targets appear (error=0). It is worth noting that although the performance of the proposed method is degraded for other values of the parameters D and τ, however, it still outperforms the conventional CS algorithm in which the missed detection, true detection, and false detection metrics equal 0.225, 0.775, and 0.9, respectively, for $\tau = 0.05$.

The receiver operating characteristic (ROC) curve for the proposed M-CS and the conventional CS algorithms (for two different values of the parameter α) are demonstrated in Fig. 6 to better evaluate and compare their performances. To obtain the ROC curves, we consider two classes of target and non-target; the target class includes 40 point targets that are distributed along the simulated speckled region. Also, the non-target class includes all the imaging points except 40 point targets. By using the proposed method, the false detection ratio is low (equal or close to zero) even for smaller values of τ. This is due to the fact the M-CS algorithm suppresses the noise level significantly, and therefore, the probability of identifying the spurious pint targets due to the presence of the noisy region will be reduced. Also, for a wide range of values of the parameter τ, most of the point targets are identified. Therefore, the obtained ROC curve is favorable, as demonstrated in Fig. 6 (a). In contrast, the probability of identifying spurious point targets increases by using the conventional CS algorithm; as a smaller value is assigned to the parameter α, a higher level of noise remains in the reconstructed image which results in increasing the false detection ratio. Also, for higher values of α, the probability of identifying the actual point targets decreases since they are removed from the reconstructed image, as previously shown. By comparing the ROCs of the conventional CS for two different values of α with the one obtained from the M-CS algorithm, the superiority of the proposed method will be concluded.

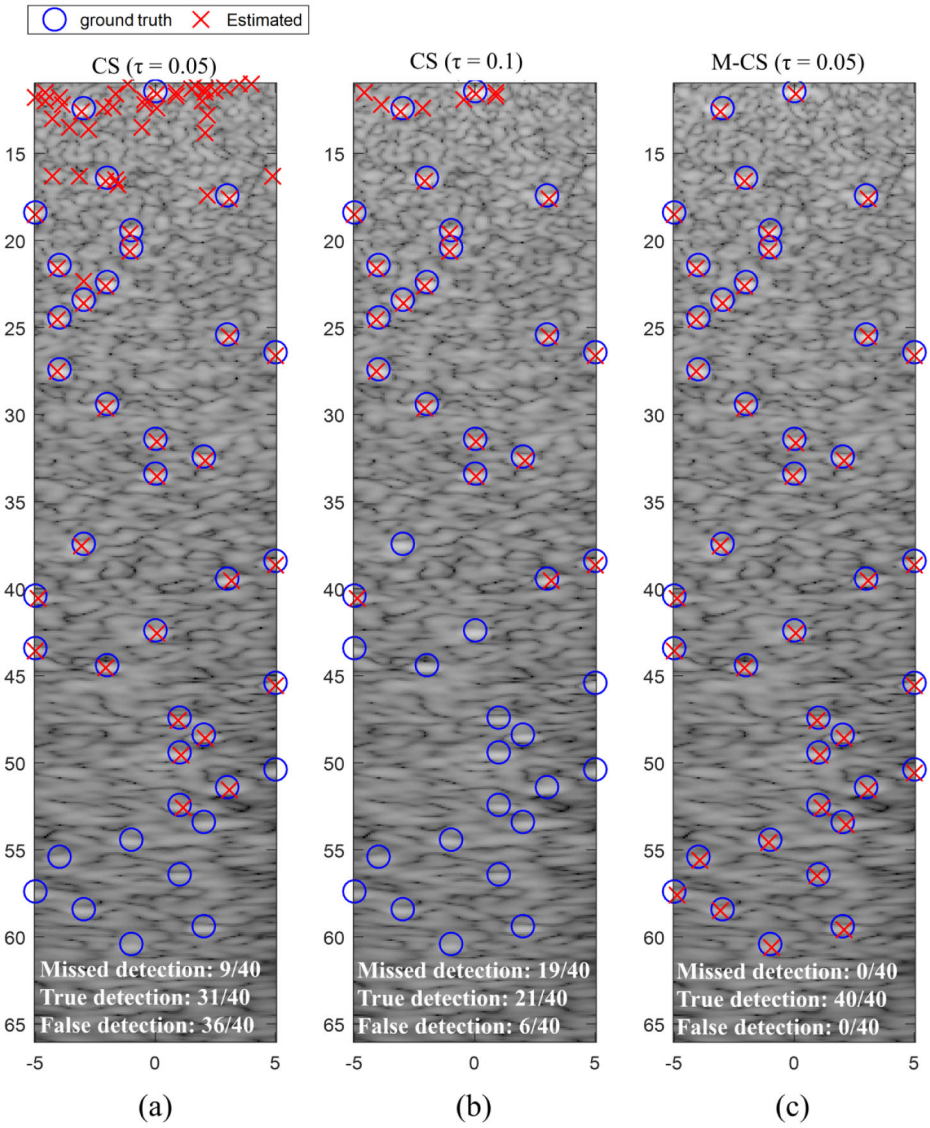

FIGURE 3. Point detection obtained from (a),(b) the CS algorithm ($\alpha = 0.1$) using two different values of τ, and (c) the M-CS algorithm ($\alpha = 1$) using $\tau = 0.05$. The images on which the identified point targets are overlaid, are shown with the dynamic range of 70 *dB*.

B. EFFECT OF THE PARAMETER α

It has been shown in Figs. 2 and 3 that the performance of the CS algorithm significantly changes for different values of α. It is desired to evaluate the proposed M-CS algorithm for different values of this parameter; Figure 7 shows the graph corresponding to the evaluation metrics for different values of α. The parameter D equals 8 in this figure. Note that for different values of α, the parameter τ changes appropriately; as the value of the parameter α decreases, a greater value is assigned to τ. This is due to the fact that the noise suppression is degraded for smaller values of α. Therefore, the threshold τ needs to be a greater value in order to filter out the noise-contaminated image and separate the point targets from the background speckle. A similar conclusion has also been made from Fig. 3 (a),(b). It can be seen from Fig. 7 that the sensitivity of the proposed algorithm to the parameter α is much less compared to the conventional CS algorithm (the results of which are shown in Figs. 2(c)-(e)). Also, all of the existing point targets are identified for different values of α while the error decreases compared to the CS algorithm (missed detection=0, and false detection$<$0.05 for all cases according to Fig. 7).

V. DISCUSSION

The proposed M-CS algorithm in PWI improves the point identification process compared to the conventional CS algorithm. The main application of the proposed method is to identify point targets, such as kidney stones, microcalcifications, and microbubbles in super-resolution imaging. A distinct feature of the proposed method compared to other

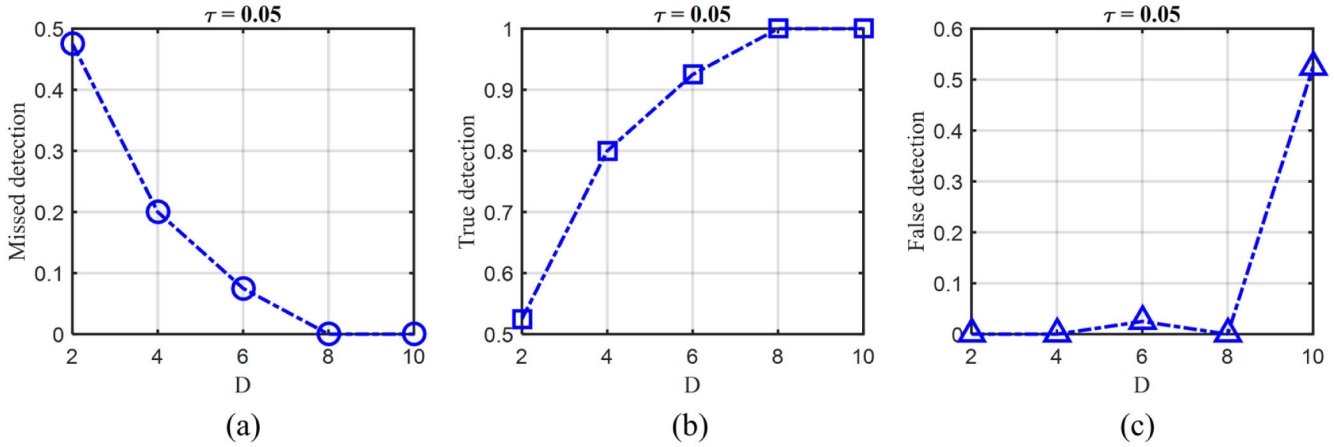

FIGURE 4. (a) Missed detection, (b) true detection, and (c) false detection evaluation metrics of the proposed method for different values of D.

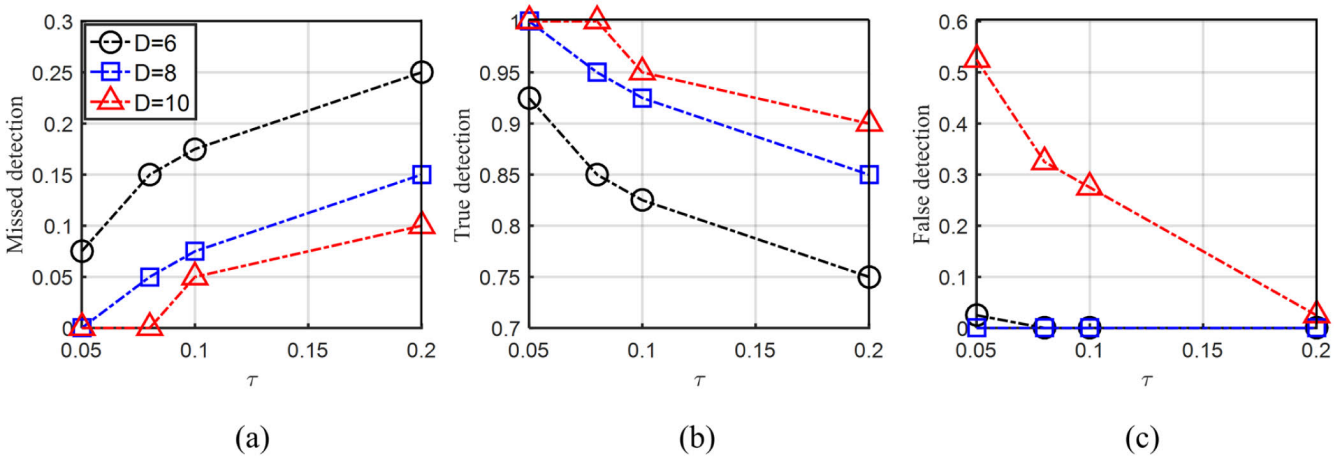

FIGURE 5. Evaluation of the proposed method for different values of τ in terms of (a) missed detection, (b) true detection, and (c) false detection evaluation metrics.

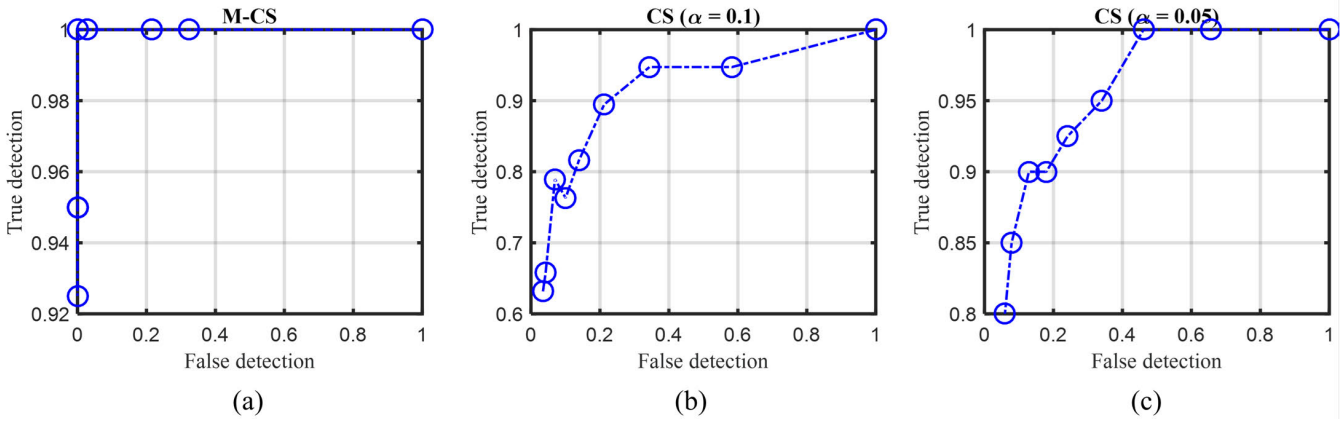

FIGURE 6. ROC curve for (a) M-CS, (b) CS with $\alpha = 0.1$, and (c) CS with $\alpha = 0.05$. $D = 8$ is considered for the proposed M-CS algorithm.

methods associated with the considered application is the successful identification of point targets in deep regions of the medium. In addition, since the proposed method is performed on PWI in which only a single emission is used, high-speed identification of point targets will be provided. Inspired by these two mentioned properties (imaging the deep

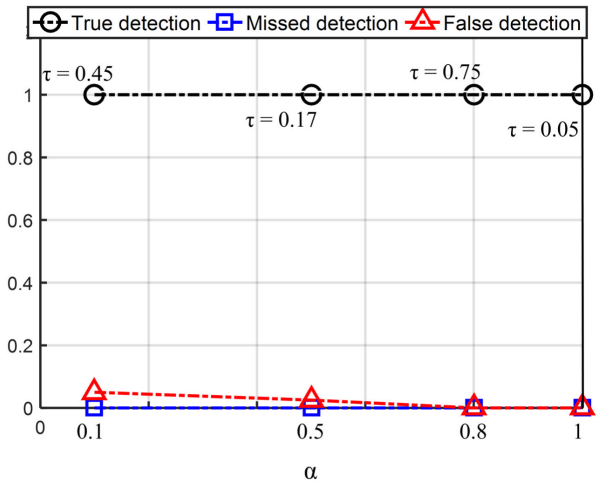

FIGURE 7. Evaluation of the proposed method for different values of the parameter α. For each value of the parameter α, the corresponding threshold value is also changed appropriately.

regions and high-speed process) of the proposed method, real-time imaging of the internal organs of the human body, with the goal of point target identification, will be achieved. Identifying the point targets using the CS algorithm imposes errors due to the limitation caused by the parameter α; the point targets that are located in deeper regions of the imaging medium are lost for larger values of α. It can be seen from Fig. 2 (e). Also, for a smaller α, the number of spurious point targets, or equivalently, the false detection metric will be increased, as demonstrated in Fig. 3 (a). The reason is that the noisy regions in the reconstructed image also pass through the threshold, and therefore, lead to the identification of some spurious point targets in the next step, i.e., the localization process. One may think that this limitation will be overcome by varying the threshold value; the identification process using a higher value of the parameter τ is also evaluated and the result is presented in Fig. 3 (b). It can be seen that the number of spurious point targets decreases by increasing the threshold value. However, this is achieved by losing the point targets that are located in deep regions; the intensity of the reconstructed point targets reduces as the imaging depth increases. This can also be qualitatively seen from Fig. 2 (d), for instance. Therefore, they will be removed similarly to the noisy regions around the point targets in the upper region of the imaging medium. By using the proposed method, these limitations will be overcome; the imaging region is divided into D parts, which are treated as D separate images to be reconstructed. Therefore, intensity reduction of the point targets by increasing the imaging depth is prevented. Also, due to the division process, one can increase the value of the parameter α in order to suppress the noise level more efficiently and identify the point targets more successfully. The greater the value of the parameter α, the better the identification, since the noise level is suppressed more successfully. This is achieved without any considerable trade-offs such as missing the deeper point targets using the proposed M-CS algorithm, which makes it advantageous over the conventional CS method. It can also be seen from Fig. 7 that no point targets are missed as the value of α increases. One should note that in order to achieve the best performance of the M-CS algorithm, the parameter τ should be selected appropriately. According to Fig. 5, it has been concluded that as the parameter D increases, the threshold value τ is desired to be increased. Also, for smaller values of α, a greater value should be assigned to the parameter τ in order to better filter out the reconstructed image and separate the point targets. Generally, since the greater value of α results in a better noise reduction, the greatest possible value of this parameter is of interest.

Note that overlaying the positions of the identified point targets on the B-mode image which is obtained from the CPWC, is to get information about the status of the point targets within the tissue (such as the distribution of microcalcifications, or the location of a stone in the kidney). Therefore, fewer emissions can also be used to obtain the B-mode image. More precisely, the number of emissions to obtain the B-mode image does not affect the accuracy of the point targets identification, since the identification process relies on using only the middle emission.

In addition to the improved accuracy in terms of the point detection process, another advantage of the proposed M-CS algorithm compared to the conventional CS method is its lower computational complexity and memory requirement; the process is independently performed on D number of sub-matrices with the size of $M \times N_x N_y/D$ using the M-CS algorithm. This is while the CS algorithm is applied to a $M \times N_x N_y$ matrix, the entries of which are D times greater compared to the one that is considered in the M-CS algorithm. Therefore, the need for memory is increased in the CS algorithm. This can cause serious problems as the imaging size (equivalently, $N_x \times N_y$) is increased. Moreover, due to the fact that smaller sub-matrices are considered in the M-CS algorithm, the process will be sped up compared to the CS algorithm. The computational time of the proposed method for different values of the parameter D (using the pre-determined measurement matrix/sub-matrices) is listed in Table 4 using a PC with the core i7-5820k CPU and 64 GB memory. It can be concluded that the processing speed of the M-CS algorithm is reduced for all values of D compared to the CS method, the computational time of which equals 64.46 seconds. Note that no parallel processing is performed in computing the proposed M-CS algorithm.

Finally, it is worth noting that in [32], a block CS algorithm was proposed and used in the image processing field to improve the processing steps compared to the conventional CS algorithm. The principles of the algorithm presented in the mentioned study differ from the proposed M-CS algorithm. To better understand the differences between these two CS-based methods, pay attention to the following explanations. In the mentioned study, the image is divided into $B \times B$ blocks in both lateral and axial directions, and a measurement matrix is defined for each block. The independent and

identically distribution (i.i.d) Gaussian matrix is considered as the measurement matrix for each block. Moreover, the samples corresponding to each block are also divided to construct that block; if the total number of samples equals M, the block CS method uses $\frac{MB^2}{N_xN_y}$ samples associated with each block ($M \ll N_xN_y$). Note that the block CS algorithm does not improve the image quality. In contrast, the division process is completely different in the proposed M-CS algorithm; consider the reconstructed image as the vector form with the dimensions of $N_xN_y \times 1$. In each step, $1/D$ part of the mentioned vector is constructed, meaning that the considered blocks in the M-CS method are not necessarily square blocks with equal dimensions in both lateral and axial directions. Also, in the proposed method, the measurement matrix is not defined for each divided part separately. Rather, one measurement matrix (which is not i.i.d) is constructed according to (4), and the result is divided into D parts. A very important difference between the proposed method and one proposed in [32], is that all of the samples in the received signal are considered to obtain the reconstructed image for each part (from 1 to D). This is due to the fact that in ultrasound imaging, the echoes reflected from all the imaging regions affect each other. This is in contrast to image processing principles, where such a relationship does not exist and each pixel has its own independent value.

TABLE 4. Computational time of the M-CS algorithm for different values of the parameter *D*.

D	3	4	5	6	8
Time (sec)	21.66	16.37	13.23	11.10	8.43

VI. CONCLUSION

In this paper, the M-CS algorithm was presented with the aim of identifying the point targets in PWI. In the proposed algorithm, the processing matrix is divided into a number of sub-matrices, each of which is processed separately. It was shown that by performing the division process, the information loss in deeper regions of the imaging object that occurs in the conventional CS algorithm is prevented. As a result, without eliminating the point targets in deep regions, larger values of the parameter α can be used to better suppress the noise level and reduce the probability of identifying the spurious point targets. Once the reconstruction is performed using the M-CS algorithm, the obtained output is thresholded and localized to achieve the positions of the point targets. The simulation results showed that the proposed algorithm successfully identifies the point targets in the highly speckle-generating medium. In addition, the processing speed increases compared to the CS algorithm. Evaluating the performance of the M-CS algorithm on the experimental data will be our future work.

CONFLICTS OF INTEREST

None Declared.

REFERENCES

[1] T. L. Szabo, *Diagnostic Ultrasound Imaging: Inside Out*. Cambridge, MC, USA: Academic, 2004.

[2] P. A. Hernández, T. T. Estrada, A. L. Pizarro, M. D. Cisternas, and C. S. Tapia, "Breast calcifications: Description and classification according to BI-RADS 5th edition," *Rev. Chil. Radiol*, vol. 22, pp. 80–91, Jan. 2016.

[3] Y. Ouyang, Z. Zhou, W. Wu, J. Tian, F. Xu, S. Wu, and P.-H. Tsui, "A review of ultrasound detection methods for breast microcalcification," *Math. Biosci. Eng.*, vol. 16, pp. 1761–1785, Mar. 2019.

[4] S. H. Thon, R. E. Hansen, and A. Austeng, "Detection of point scatterers in medical ultrasound," *IEEE Trans. Ultrason., Ferroelectr., Freq. Control*, vol. 69, no. 2, pp. 617–628, Feb. 2022.

[5] R. Tasbaz and B. M. Asl, "Improvement of microbubbles localization using adaptive beamforming in super-resolution ultrasound imaging," in *Proc. IEEE Int. Ultrason. Symp. (IUS)*, Sep. 2021, pp. 1–4.

[6] J.-F. Synnevag, A. Austeng, and S. Holm, "Benefits of minimum-variance beamforming in medical ultrasound imaging," *IEEE Trans. Ultrason., Ferroelectr., Freq. Control*, vol. 56, no. 9, pp. 1868–1879, Sep. 2009.

[7] B. M. Asl and A. Mahloojifar, "Contrast enhancement and robustness improvement of adaptive ultrasound imaging using forward-backward minimum variance beamforming," *IEEE Trans. Ultrason., Ferroelectr., Freq. Control*, vol. 58, no. 4, pp. 858–867, Apr. 2011.

[8] B. M. Asl and A. Mahloojifar, "Eigenspace-based minimum variance beamforming applied to medical ultrasound imaging," *IEEE Trans. Ultrason., Ferroelectr., Freq. Control*, vol. 57, no. 11, pp. 2381–2390, Nov. 2010.

[9] S. Mehdizadeh, A. Austeng, T. F. Johansen, and S. Holm, "Eigenspace based minimum variance beamforming applied to ultrasound imaging of acoustically hard tissues," *IEEE Trans. Med. Imag.*, vol. 31, no. 10, pp. 1912–1921, Oct. 2012.

[10] S.-L. Wang, C.-H. Chang, H.-C. Yang, Y.-H. Chou, and P.-C. Li, "Performance evaluation of coherence-based adaptive imaging using clinical breast data," *IEEE Trans. Ultrason., Ferroelectr., Freq. Control*, vol. 54, no. 8, pp. 1669–1679, Aug. 2007.

[11] T. Szasz, A. Basarab, and D. Kouamé, "Strong reflector-based beamforming in ultrasound medical imaging," *Ultrasonics*, vol. 66, pp. 111–124, Mar. 2016.

[12] T. Szasz, A. Basarab, M.-F. Vaida, and D. Kouamé, "Beamforming with sparse prior in ultrasound medical imaging," in *Proc. IEEE Int. Ultrason. Symp.*, Sep. 2014, pp. 1077–1080.

[13] S.-W. Huang, J.-L. Robert, E. Radulescu, F. Vignon, and R. Erkamp, "Beamforming techniques for ultrasound microcalcification detection," in *Proc. IEEE Int. Ultrason. Symp.*, Sep. 2014, pp. 2193–2196.

[14] S. M. Hverven, O. M. H. Rindal, A. J. Hunter, and A. Austeng, "Point scatterer enhancement in ultrasound by wavelet coefficient shrinkage," in *Proc. IEEE Int. Ultrason. Symp. (IUS)*, Sep. 2017, pp. 1–4.

[15] M. Bilodeau, N. Quaegebeur, A. Berry, and P. Masson, "Correlation-based ultrasound imaging of strong reflectors with phase coherence filtering," *Ultrasonics*, vol. 119, Feb. 2022, Art. no. 106631.

[16] G. Matrone, M. A. L. Bell, and A. Ramalli, "Spatial coherence beamforming with multi-line transmission to enhance the contrast of coherent structures in ultrasound images degraded by acoustic clutter," *IEEE Trans. Ultrason., Ferroelectr., Freq. Control*, vol. 68, no. 12, pp. 3570–3582, Dec. 2021.

[17] S. H. Thon, R. E. Hansen, and A. Austeng, "Point detection in ultrasound using prewhitening and multilook optimization," *IEEE Trans. Ultrason., Ferroelectr., Freq. Control*, vol. 69, no. 6, pp. 2085–2097, Jun. 2022.

[18] J. E. Tierney, S. G. Schlunk, R. Jones, M. George, P. Karve, R. Duddu, B. C. Byram, and R. S. Hsi, "In vitro feasibility of next generation non-linear beamforming ultrasound methods to characterize and size kidney stones," *Urolithiasis*, vol. 47, no. 2, pp. 181–188, Apr. 2019.

[19] M. Yousufi, M. Amir, U. Javed, M. Tayyib, S. Abdullah, H. Ullah, I. M. Qureshi, K. S. Alimgeer, M. W. Akram, and K. B. Khan, "Application of compressive sensing to ultrasound images: A review," *BioMed Res. Int.*, vol. 2019, pp. 1–14, Nov. 2019.

[20] C. Wang, X. Peng, D. Liang, and H. Zheng, "Plane-wave ultrasound imaging based on compressive sensing with low memory occupation," in *Proc. IEEE Int. Ultrason. Symp. (IUS)*, Oct. 2015, pp. 1–4.

[21] H. Liebgott, R. Prost, and D. Friboulet, "Pre-beamformed RF signal reconstruction in medical ultrasound using compressive sensing," *Ultrasonics*, vol. 53, no. 2, pp. 525–533, Feb. 2013.

[22] R. Paridar and B. M. Asl, "Plane wave ultrasound imaging using compressive sensing and minimum variance beamforming," *Ultrasonics*, vol. 127, Jan. 2023, Art. no. 106838.
[23] M. F. Schiffner, T. Jansen, and G. Schmitz, "Compressed sensing for fast image acquisition in pulse-echo ultrasound," *Biomed. Eng. Biomedizinische Technik*, vol. 57, Aug. 2012, Art. no. 000010151520124142.
[24] M. Tanter and M. Fink, "Ultrafast imaging in biomedical ultrasound," *IEEE Trans. Ultrason., Ferroelectr., Freq. Control*, vol. 61, no. 1, pp. 102–119, Jan. 2014.
[25] M. Fink, "Time reversal of ultrasonic fields. I. Basic principles," *IEEE Trans. Ultrason., Ferroelectr., Freq. Control*, vol. 39, no. 5, pp. 555–566, Sep. 1992.
[26] G. Montaldo, M. Tanter, J. Bercoff, N. Benech, and M. Fink, "Coherent plane-wave compounding for very high frame rate ultrasonography and transient elastography," *IEEE Trans. Ultrason., Ferroelectr., Freq. Control*, vol. 56, no. 3, pp. 489–506, Mar. 2009.
[27] M. Shen, Q. Zhang, D. Li, J. Yang, and B. Li, "Adaptive sparse representation beamformer for high-frame-rate ultrasound imaging instrument," *IEEE Trans. Instrum. Meas.*, vol. 61, no. 5, pp. 1323–1333, May 2012.
[28] E. Ozkan, V. Vishnevsky, and O. Goksel, "Inverse problem of ultrasound beamforming with sparsity constraints and regularization," *IEEE Trans. Ultrason., Ferroelectr., Freq. Control*, vol. 65, no. 3, pp. 356–365, Mar. 2018.
[29] Y. Zhang, Y. Wang, and C. Zhang, "Efficient discrete cosine transform model–based algorithm for photoacoustic image reconstruction," *J. Biomed. Opt.*, vol. 18, no. 6, Jun. 2013, Art. no. 066008.
[30] R. Paridar, M. Mozaffarzadeh, V. Periyasamy, M. Pramanik, M. Mehrmohammadi, and M. Orooji, "Sparsity-based beamforming to enhance two-dimensional linear-array photoacoustic tomography," *Ultrasonics*, vol. 96, pp. 55–63, Jul. 2019.
[31] J. A. Jensen, "Field: A program for simulating ultrasound systems," in *Proc. 10th Nordicbaltic Conf. Biomed. Imag.*, vol. 4, Jan. 1996, pp. 351–353.
[32] L. Gan, "Block compressed sensing of natural images," in *Proc. 15th Int. Conf. Digit. Signal Process.*, Jul. 2007, pp. 403–406.

ROYA PARIDAR received the M.Sc. degree in biomedical engineering from Tarbiat Modares University, Tehran, Iran, in 2019, where she is currently pursuing the Ph.D. degree in biomedical engineering. Her research interests include medical signal processing, ultrafast imaging, and beamforming.

BABAK MOHAMMADZADEH ASL (Member, IEEE) is currently an Associate Professor in biomedical engineering with Tarbiat Modares University (TMU). He is also an Associate Dean of Research with the Faculty of Electrical and Computer Engineering. His research interests include medical ultrasound within the areas of beamforming and array signal processing. Specifically, the focus of his research has been on the implementation of adaptive beamforming methods in ultrasound imaging and vector flow imaging and solving the limitations and requirements of applying these methods in the field of medical ultrasound. He has been worked continuously in this field, since 2006, and supervised nine Ph.D. students and 50 M.Sc. students. He has awarded as a Distinguished Researcher and a Distinguished Professor of TMU, in 2017 and 2019, respectively, and a Distinguished Professor in education of TMU, in 2020. According to the Stanford's list of world's top 2% most-cited scientists, in 2022, he ranked among the top 2% of highly cited scientists.